Nanotechnology

PAPER

Predictable and adjustable broadband gold nanorods for photothermal effects and foldable performances

To cite this article: Xi Chen *et al* 2024 *Nanotechnology* **35** 115701

IOP Publishing Nanotechnology
Nanotechnology **35** (2024) 115701 (10pp) https://doi.org/10.1088/1361-6528/ad1445

Predictable and adjustable broadband gold nanorods for photothermal effects and foldable performances

Xi Chen, Jie Liu*, Xun Li, Zhiqun Cheng and Tian-Song Deng*

School of Electronics and Information Engineering, Hangzhou Dianzi University, Hangzhou 310018,
People's Republic of China

E-mail: dengts@pku.edu.cn and liujie4209@hdu.edu.cn

Received 22 August 2023, revised 26 November 2023
Accepted for publication 10 December 2023
Published 27 December 2023

Abstract

Colloidal gold nanorods (GNRs) have demonstrated their potential to absorb light within specific wavelength bands and induce photothermal effects. However, the unpredictability and lack of adjustability in the broadband spectrum formed by the self-assembly of gold nanospheres or the coupling of various sizes of GNRs have posed significant challenges. To address this, we have developed broadband GNRs (BGNRs) with a predictable and adjustable extinction band in the visible and near-infrared regions. The BGNRs were synthesized by simply mixing GNRs with different aspect ratios, allowing for control over the bandwidths and positions of the extinction bands. Subsequently, the BGNRs were coated with silica and underwent surface modification. The resulting BGNRs@SiO_2 were then mixed with either polydimethylsiloxane (PDMS) or polyvinylidene fluoride (PVDF) to create BGNRs@SiO_2/PDMS (or PVDF) films. The BGNRs@SiO_2/PDMS and BGNRs@SiO_2/PVDF films both exhibit excellent photothermal performance properties. Additionally, the light absorption intensity of the BGNRs@SiO_2/PVDF film linearly increases upon folding, leading to significantly enhanced photothermal performance after folding. This work demonstrates that plasmonic colloidal GNRs, without the need for coupling, can yield predictable and adjustable extinction bands. This finding holds great promise for future development and practical applications, particularly in the transfer of these properties to films.

Supplementary material for this article is available online

Keywords: gold nanorods, broadband, PDMS film, PVDF film, photothermal effects

Introduction

In recent decades, gold nanorods (GNRs) have garnered significant attention due to their intriguing localized surface plasmon resonance (LSPR) characteristics, which can be adjusted based on the aspect ratio (AR) of the GNRs [1–10]. These properties have found applications in various fields such as synthesis [11–13], self-assembly [14–16], cancer treatment [17–19], and photocatalysis [20–22]. However, the low photothermal conversion efficiency of narrow-band GNRs poses challenges in meeting the demands of solar energy conversion and photocatalysis for optical devices and nanomedicine applications [23, 24]. On the other hand, GNRs with broadband light-absorbing properties have been extensively utilized in solar energy conversion [25–27], photothermal effects [28–30], and the fabrication of novel optoelectronic devices [31, 32]. Consequently, there is a growing interest among researchers in developing broadband light-absorbing GNRs with excellent solar energy conversion characteristics and photocatalytic properties.

To address the issue of narrowband characteristics, researchers have developed broadband nanostructures using gold nanoparticles. For instance, Xiang *et al* [33] mixed GNRs of three different sizes and deposited them on a glass sheet to create

---

[*] Authors to whom any correspondence should be addressed.

a film with broadband properties. They then placed GNRs on Pt electrodes for near-infrared and short-wave infrared broadband photoelectric detection. The coupling effect between GNRs led to a broad plasmonic band ranging from 400 to 2000 nm in the thin film. However, the coupling of GNRs introduces randomness, making the obtained plasmonic band unpredictable. In another study, Nayoung Kwon *et al* [34] developed a method to form self-assembled colloidal superparticles with a broadband range of 400 nm–2.5 μm. These gold superparticles exhibited excellent performance in near-infrared surface-enhanced Raman spectroscopy and light-to-heat conversion due to their broadband properties. However, the bandwidth of these superparticles is predetermined during preparation and cannot be adjusted according to specific requirements. While there have been advancements in material synthesis and the optical effects resulting from the plasmonic coupling of GNRs or the self-assembly of gold nanoparticles into superparticles, achieving a predictable plasmonic band with an adjustable bandwidth remains a significant challenge which has been rarely explored.

In this study, we present a method for preparing BGNRs and their films with adjustable and predictable plasmonic bands. Our approach involves several steps. Firstly, we mixed colloidal GNRs with varying aspect ratios, enabling us to achieve a plasmonic bandwidth ranging from 600 to over 1100 nm. This was accomplished by adjusting the mixing ratio and utilizing different types of GNRs. Secondly, after silica coating and surface modification, polydimethylsiloxane (PDMS) and polyvinylidene fluoride (PVDF) films composed of BGNRs were prepared. Since the GNRs were separated by the silica shell, the plasmonic coupling between GNRs could be neglected. Thus, the spectra of BGNRs/PDMS and BGNRs/PVDF films could be arbitrarily adjusted and predicted by the LSPRs of BGNRs. Both BGNRs@SiO_2/PDMS films and BGNRs@SiO_2/PVDF films exhibited excellent photothermal performance in the ethanol solution temperature change tests. Moreover, the spectra of BGNRs@SiO_2/PVDF films showed a linear change during folding, directly proportional to the number of folds. After folding, the photothermal performance of BGNRs@SiO_2/PVDF films significantly improved. We also conducted an investigation into the impact of film thickness on photothermal performance, conclusively establishing that particles were the primary reason for the outstanding photothermal performance. Finally, FDTD simulations were performed, and found the coupling effect between the GNRs could be neglected when the GNRs were covered by a silica shell. This work provides a way to prepare BGNRs and their films with predictable and adjustable LSPR bands, which can be extended to other nanoparticle systems.

Experimental section

Materials

All chemicals were obtained from commercial suppliers and used without further purification. Hexadecyltrimethylammonium bromide (CTAB > 99.0%), chloroauric acid ($HAuCl_4$), L-ascorbic acid (AA > 99.99%), and octadecyltrimethoxysilane (OTMS, 90%) were purchased from Shanghai Macklin Biochemical Technology Co., Ltd. Silver nitrate ($AgNO_3 > 99.8\%$), sodium oleate (NaOL > 99.88%), sodium borohydride ($NaBH_4$ > 98%), 1-Methyl-2-pyrrolidinone (NMP > 99%), and tetraethylorthosilicate (TEOS, 99.99%) were purchased from Shanghai Aladdin Biochemical Technology Co., Ltd. Sodium hydroxide (NaOH), ethanol, and aqueous ammonia were purchased from Hangzhou Gaojing Chemical Co., Ltd. Sylgard 184 polydimethylsiloxane (PDMS) elastomer base and curing agents were obtained from Dow Corning Corporation. The Polyvinylidene Fluoride (PVDF) (HSV 900) was purchased from Beijing Saibo Electrochemical Materials Co., Ltd. All glassware were cleaned using freshly prepared aqua regia (HCl:HNO_3 in a 3:1 ratio by volume) followed by rinsing with copious amounts of water. Ultrapure water with a resistivity of 18.2 MΩ was used in all of the experiments.

Preparation of BGNRs@SiO_2

Prior to the preparation, GNRs of various types that were previously synthesized (500 ml) underwent centrifugation at 7000 rpm for 30 min, followed by the removal of the supernatant [1]. The resulting precipitate was re-dispersed in deionized (DI) water and subjected to another round of centrifugation. Subsequently, the precipitate was re-dispersed in a CTAB solution (200 ml, 1.5 mM). The GNRs were then ranked as a-f based on their LSPRs, ranging from 690 to 1090 nm. The mixing ratio of GNRs was adjusted to achieve a proportion of 3.5:1.2:2:2.5:1.2:3 for GNRs a-f, respectively. Once the GNRs were mixed in the designated proportions (total volume of 100 ml), the solution was subjected to ultrasonic treatment for two minutes, resulting in a mixed solution exhibiting broadband properties.

Meso-SiO_2 coating

The BGNRs solution (100 ml) was subjected to magnetic stirring (400 rpm), and then a 0.1 M NaOH solution (1.0 ml) was added. Following this, three additions of a TEOS solution (20 v% in ethanol, 0.3 ml) were made at 1 h intervals. The reaction was allowed to proceed for one day with continuous stirring to produce BGNRs@SiO_2. Afterward, the resulting particles were centrifuged at 7000 rpm in a mixture of water and ethanol for 10 min. Finally, they were dispersed in ethanol (100 ml) for subsequent experiments.

Surface modification

To disperse the BGNRs@SiO_2 in an organic solvent for subsequent experiments, we employed a previously described surface modification method with minor modifications [35], which was performed by hydrophobating the silica surfaces using a silane coupling agent called Octadecyltrimethoxysilane (OTMS). Initially, 1 ml of NH_4OH (32%) was dropwise added to 100 ml of BGNRs@SiO_2 in ethanol while vigorously stirring. Subsequently, 10 ml of OTMS (2.4 wt% in chloroform) was added to the solution. The mixture was left to react for 24 h. Then, the solution was centrifuged twice with ethanol at 7000 rpm for 10 min. Following this, it was centrifuged once with either toluene or NMP solution. Finally, the particles were dispersed in toluene or NMP for further experimentation.

PDMS films

Polydimethylsiloxane (PDMS) was employed as the polymer layer. A solution containing a mixture of PDMS elastomer base, curing agent, and BGNRs@SiO$_2$ solution in a mass ratio of 10:1:5 was dispensed into a 20 ml glass bottle. The solution was thoroughly mixed and subsequently poured into a glass culture dish with a diameter of 6 cm to form a film. To eliminate any air bubbles trapped in the PDMS, the dish was placed in a vacuum chamber for 1 h. Finally, the film was heated at 90 °C overnight.

PVDF films

A homogeneous dope solution was prepared by dissolving 10 wt% PVDF powder in NMP solvent at 60 °C with continuous stirring. The solution was then allowed to stand still at 50 °C for 12 h to facilitate degassing. Subsequently, the degassed PVDF solution was mixed with the BGNRs@SiO$_2$ solution at a volume ratio of 1:1. The resulting mixture was uniformly coated onto a glass slide and left at 50 °C overnight to allow for the formation of the PVDF film.

Characterizations

Optical extinction spectra were recorded with a UV-1900i spectrophotometer (Shimadzu, Japan) with a 10 mm optical path. Transmission electron microscopy (TEM) images were obtained with a HT-7700 microscope (Hitachi, Japan) operating at 100 kV. Infrared images are taken by high-definition infrared thermometer (Hikmicro, China) at room temperature. A 350 W Xenon lamp (HDL-II, Suzhou Betical Optoelectronics Technology Co., Ltd, China) was used as the light source, equipped with a filter which the light wavelength less than 420 nm was cut off.

The synthesis schematic diagram of BGNRs@SiO$_2$/PDMS films

Scheme 1 illustrates the synthesis schematic diagram of the BGNRs@SiO$_2$/PDMS film. The following steps were involved in the preparation: GNRs with various localized surface plasmon resonances (LSPRs) were synthesized using a seed-mediated growth method.[1] Gernerally, seed-mediated growth involves the synthesis of GNRs by adding a seed solution, which has been synthesized and aged for thirty minutes, into a pre-prepared growth solution. The modulation of GNRs' LSPR peaks can be achieved by adjusting factors such as the seed quantity, pH value, and the amount of AgNO$_3$ in the growth solution. The extinction spectra data of the synthesized GNRs were imported into Origin software for analysis. The proportion of six different types of GNRs required for BGNRs preparation was calculated based on the extinction spectra data. The GNRs were mixed according to the calculated proportion to obtain BGNRs. NaOH and TEOS were added to the BGNRs solution to facilitate the deposition of a mesoporous silica shell on the surface of the GNRs. After the coating process, the BGNRs@SiO$_2$ particles were cleaned, and then ammonia and OTMS were added to exchange the surface ligands, enabling the dispersion of BGNRs@SiO$_2$ in toluene. PDMS and the curing agent were mixed in the appropriate proportion. BGNRs@SiO$_2$ were added to the PDMS mixture, and the solution was stirred until it was uniformly mixed. The mixed solution was poured into a petri dish and placed in a vacuum environment to remove air bubbles. The dish was then heated to obtain the BGNRs@SiO$_2$/PDMS films.

Results and discussion

Synthesis and characterization of BGNRs@SiO$_2$

BGNRs were obtained by mixing GNRs synthesized using binary surfactants in the appropriate proportion. TEM images and extinction spectra of the GNRs and BGNRs are shown in figure 1. The aspect ratio (AR) of the GNRs was adjustable from 2.2 to 6.9 by varying synthetic parameters such as AgNO$_3$, seed solution, and pH of the growth solution (detailed in table S1). The optical extinction spectra revealed that the GNRs exhibited narrowband LSPRs at wavelengths around 690, 760, 830, 880, 950, and 1090 nm. Due to precise control over the conditions involved in the growth process, the synthesized GNRs possessed narrowband characteristics, allowing for better modulation of the broadband plasmonic band. These six GNRs aqueous solutions were mixed in an optimized ratio to form the BGNRs solution (indicated by the black line in figure 1(h)). The shape of the extinction spectrum could be adjusted by altering the ratio of GNRs, as demonstrated in figure S1. During the solvent transfer process, direct modification of GNRs' surfaces with OTMS was not feasible. Therefore, a mesoporous silica layer was coated on the GNRs to facilitate the grafting of OTMS. The presence of the mesoporous silica layer enhanced the stability of the GNRs solution. After coating with silica, the BGNRs@SiO$_2$ could be transferred to ethanol. Subsequently, the OTMS ligand conversion rendered it oleophilic, allowing for transfer to a toluene solution. The grafting process involved the hydrolysis of methoxyl groups and the condensation of resulting silantriol with the siloxy group. Upon grafting, BGNRs@SiO$_2$ exhibited an affinity for oil, enabling their transfer to toluene [36, 37]. The corresponding photograph of the actually synthesized GNRs solution can be seen in figure S2. It is important to note that each GNR in the mixture contributed to the extinction spectra within its specific wavelength range. The presence of a mesoporous silica layer

---

[1] Seed-mediated growth involves the synthesis of GNRs by adding a seed solution, which has been synthesized and aged for thirty minutes, into a pre-prepared growth solution. The modulation of GNRs' LSPR peaks can be achieved by adjusting factors such as the seed quantity, pH value, and the amount of AgNO3 in the growth solution.

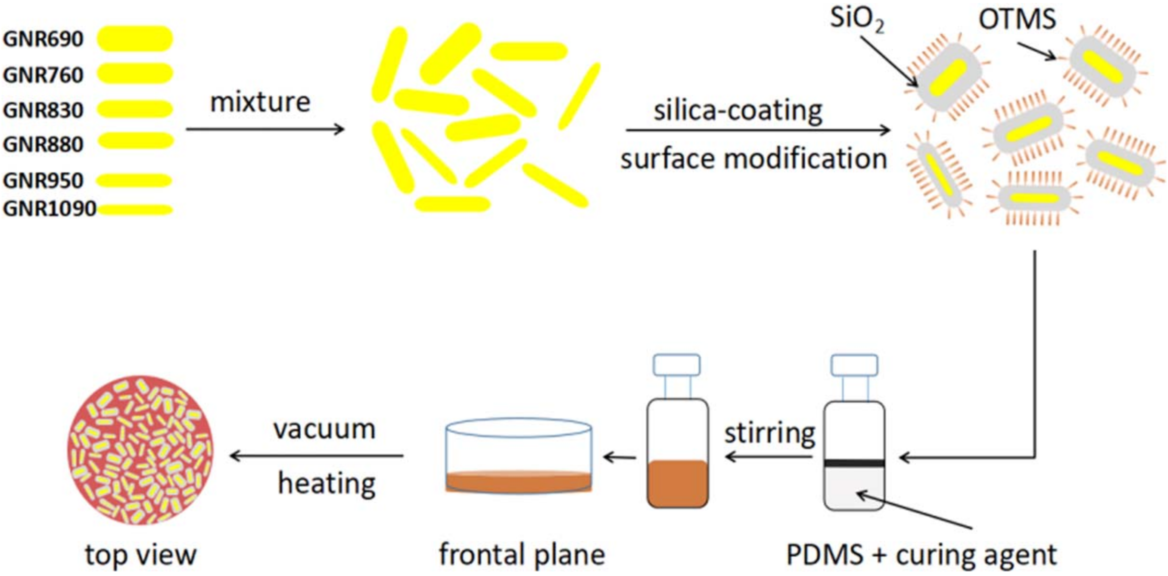

Scheme 1. Schematic diagram of synthesis, silica-coating and surface modification of broadband GNRs and fabrication of PDMS films.

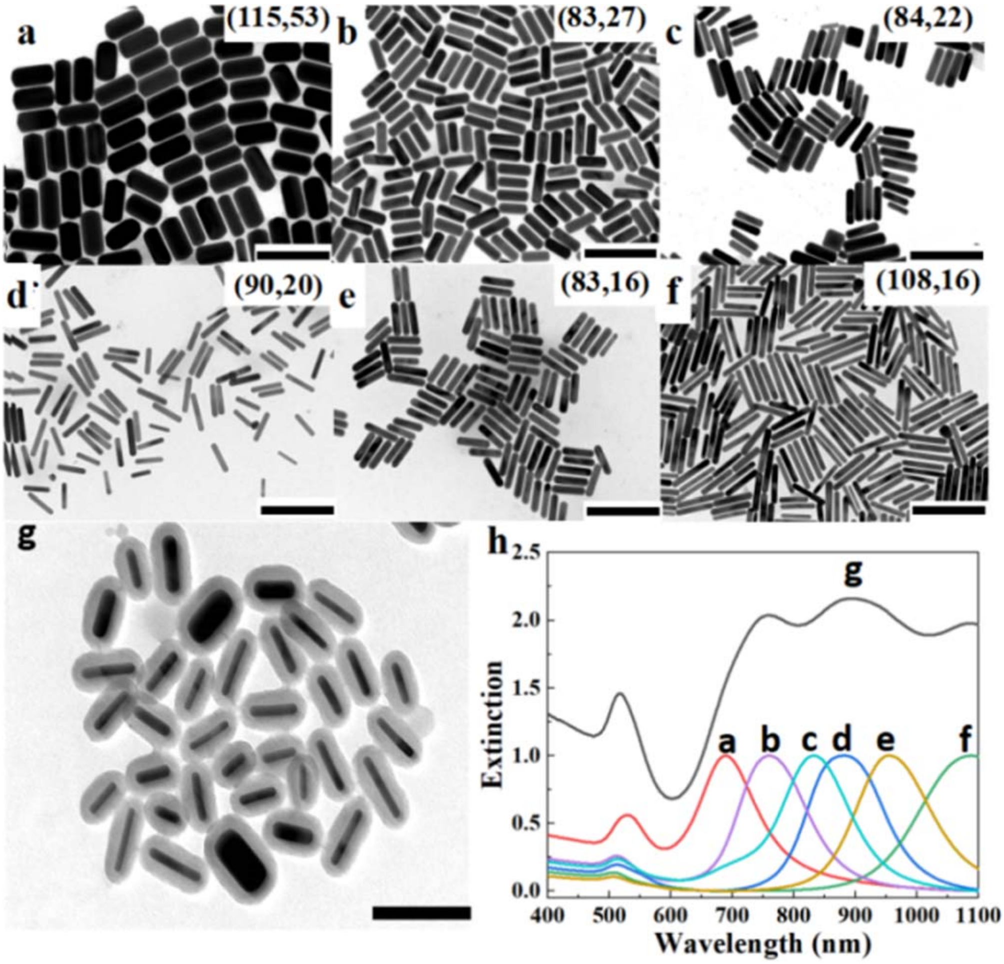

Figure 1. (a)–(f) TEM images of six GNRs with different ARs. The values on the top-right corners are the lengths and diameters of the GNRs. The AR of GNRs increase continuously from 1(a) to 1(f). (g) TEM image of BGNRs@SiO$_2$. The thickness of the mesoporous silica shell on the BGNRs surface is about 20 nm. (h) Normalized experimental extinction spectra of GNRs and extinction spectra of BGNRs@SiO$_2$. All scale bars are 200 nm.

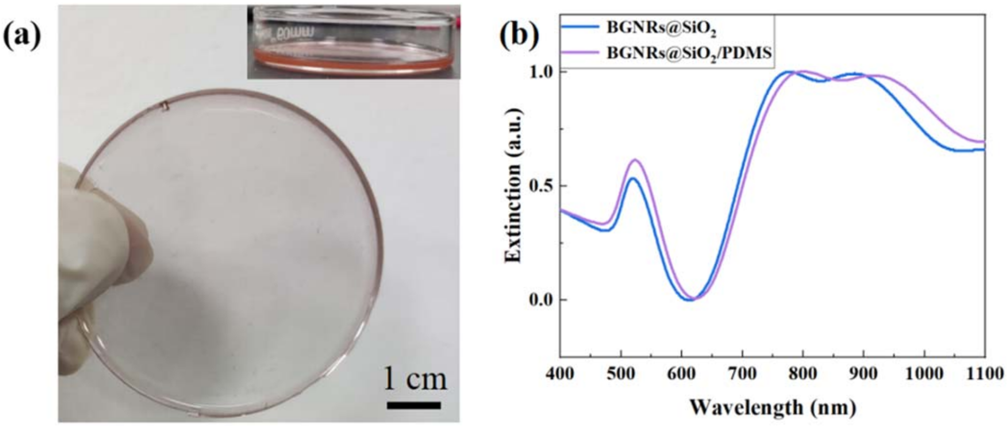

Figure 2. (a) A photograph of PDMS film which containing BGNRs@SiO$_2$ made in a 6 cm Petri dish. The inset shows the front view of the PDMS film in the petri dish. (b) Normalized extinction spectra of the BGNRs@SiO$_2$ in the toluene and in PDMS film.

and subsequent grafting with OTMS enabled the successful transfer of BGNRs@SiO$_2$ to toluene.

Synthesis and extinction spectra of the BGNRs@SiO$_2$/PDMS films

A PDMS film with a diameter of 6 cm was prepared in a Petri dish following the procedure depicted in figure S3. Prior to pouring the solution into the dish, PDMS, curing agent, and BGNRs@SiO$_2$ particles were mixed in a bottle. Stirring was performed to ensure a homogeneous mixture and to remove any bubbles present. The solution was then poured into the Petri dish and subjected to a vacuum environment for 1 h to eliminate all bubbles completely. Subsequently, the dish was heated to 90 °C and left overnight to allow the BGNRs@SiO$_2$/PDMS film to form. It is important to note that heating the film directly without prior stirring and vacuum treatment would result in an uneven film with potential holes due to the presence of bubbles, as illustrated in figure S4. The final BGNRs@SiO$_2$/PDMS film, shown in figure 2(a), exhibited a diameter identical to that of the Petri dish (6 cm). The inset of figure 2(a) provides a front view of the film in the Petri dish after being removed from the vacuum drying oven. Notably, the shape of the extinction spectra remained unchanged, indicating that the addition of BGNRs@SiO$_2$ did not affect the extinction spectrum. This finding demonstrates that the extinction spectra in the BGNRs@SiO$_2$/PDMS films can be predicted and maintained, as depicted in figure 2(b).

Photothermal performance test of BGNRs@SiO$_2$/PDMS films

As illustrated in figure 3(a), the temperature changes of the ethanol solution were utilized to reflect the photothermal performance of the BGNRs@SiO$_2$/PDMS film. The temperature changes of the ethanol solution were recorded at 20 s intervals over a 10 min period under Xenon lamp irradiation. The positions where the ethanol solution was measured with an infrared thermometer and where the BGNRs@SiO$_2$/PDMS film was placed are indicated in figure S5. In the sample bottle equipped with the BGNRs@SiO$_2$/PDMS film (figure 3(b)), the temperature of the ethanol solution increased from 19.3 °C to 23.3 °C. Conversely, in the sample bottle with the PDMS film lacking particles (figure 3(c)), under the same irradiation conditions, the temperature of the ethanol solution rose from 18.9 °C to 30.3 °C. This temperature disparity can be attributed to the photothermal effect of BGNRs@SiO$_2$. When the Xenon lamp illuminated, the plasmonic GNRs absorbed photons and converted them into thermal energy, elevating the surface temperature of the film. Simultaneously, the inherent photothermal properties of the BGNRs@SiO$_2$/PDMS film insulated heat from transferring to the ethanol solution. Consequently, the ethanol solution underneath the PDMS film with BGNRs@SiO$_2$ experienced a lower temperature increase compared to the solution under the PDMS film without particles, indicating the superior photothermal performance of BGNRs@SiO$_2$/PDMS. Additionally, the photothermal conversion capability of BGNRs@SiO$_2$ was evaluated. When exposed to a 350 W Xenon lamp for 10 min, the temperature of the dispersed BGNRs@SiO$_2$ in ethanol increased from 28.5 °C to 43.5 °C, whereas under the same irradiation conditions, the temperature of pure ethanol solution rose from 28.5 °C to 33.2 °C (figure S6). These results underscore the highly efficient photothermal conversion properties of BGNRs@SiO$_2$ as near-infrared (NIR) absorbers, consistent with the photothermal performance of the BGNRs@SiO$_2$/PDMS film.

Folding performance test of the BGNRs@SiO$_2$/PVDF films

To investigate the effect of adding particles to the PVDF film on its folding performance, a PVDF film without particles was first prepared to determine its folding behavior (figure S7). The process of preparing the BGNRs@SiO$_2$/PVDF film was similar to that of the BGNRs@SiO$_2$/PDMS film (figure S8). Initially, BGNRs@SiO$_2$ particles were transferred to an NMP solution and then mixed with the PVDF solution. The mixture was stirred and dropped onto a glass plate, which was subsequently heated at 70 °C overnight to obtain the BGNRs@SiO$_2$/PVDF film. The BGNRs used in this process were prepared by mixing five types of GNRs. Figure 4(a) shows the extinction spectra of the BGNRs transferred to the NMP solution, which exhibited some differences compared to the extinction spectra obtained from the folding test shown in figure 4(b). One of the main reasons for

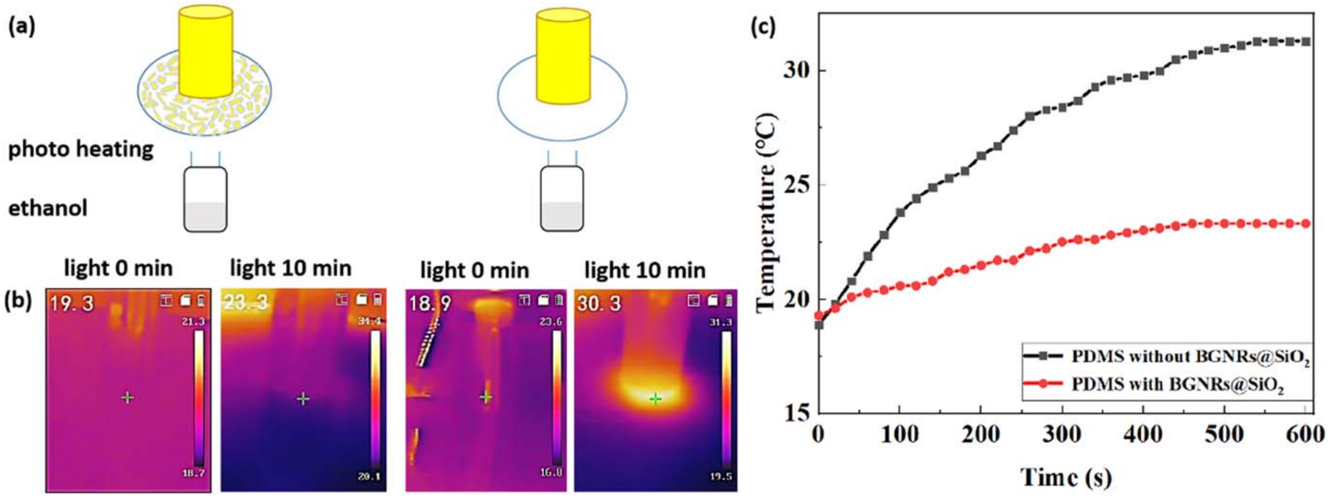

Figure 3. (a) Schematic diagram of the photothermal performance test device, which consists of Xenon lamp, PDMS film and sample bottle with ethanol solution. And the films from left to right are BGNRs@SiO_2/PDMS and pure PDMS without particles. (b) Photographs taken with a high-definition infrared thermometer to record the temperature of the ethanol solution in the sample bottle when it was irradiated by a Xenon lamp for 0 min and 10 min of irradiation. (c) Plots of temperature of ethanol under BGNRs@SiO_2/PDMS film (red) and ethanol under PDMS film (black) without nanoparticles upon irradiation 350 W Xenon lamp as a function of time.

these differences is that air was selected as the baseline for measurement in both tests. Figure 4(b) represents the extinction spectra generated by the BGNRs@SiO_2/PVDF film. The extinction spectral intensity of the PVDF film without particles gradually decreased with a red-shift in the peak position (figure S7). This explains why the original extinction spectra of the BGNRs were relatively flat, while the peak in the BGNRs@SiO_2/PVDF spectra was prominent around 740 nm. After folding, the extinction spectra of the BGNRs@SiO_2/PVDF film increased linearly with the number of folds, and this change was represented by the peak value at 740 nm. In figure 4(b), the solid line represents the actual measured extinction spectra obtained during the folding process of the BGNRs@SiO_2/PVDF film. The peak value at 740 nm was 0.3 when unfolded, increased to 0.6 after one fold. However, when folded two and three times, the peak values at 740 nm reached 1.1 and 2.1, respectively, instead of the expected values of 1.2 and 2.4 based on absolute linearity. According to the hypothesis, this discrepancy arises because the BGNRs@SiO_2/PVDF film, when folded and placed into the spectrometer, did not completely overlap (figure S9). As a result, the measured extinction values of the spectra decreased. The dashed line represents the simulated calculation obtained by multiplying the original spectra of BGNRs@SiO_2/PVDF with the corresponding factors. It can be observed that the shape of the spectra remains consistent, with only minor differences in intensity. We also conducted SEM imaging of the prepared BGNRs@SiO_2/PVDF films to observe the distribution of GNRs@SiO_2 within the matrix (figure S10). It is evident that GNRs@SiO_2 in the BGNRs@SiO_2/PVDF film are widely distributed, with distances between them generally exceeding 100 nm. This distance allows for neglective plasmonic coupling between GNRs.

Photothermal performance test of BGNRs@SiO_2/PVDF films

The method of measuring temperature changes was consistent with the approach used for evaluating the BGNRs@SiO_2/PDMS film, as mentioned earlier. Figure 4(c) illustrates the temperature variations of the ethanol solution under different conditions: unfolded and folded multiple times with BGNRs@SiO_2/PVDF films. It can be observed that as the number of folds increased, the photothermal performance of the BGNRs@SiO_2/PVDF film improved significantly. Without folding, under identical irradiation conditions, the temperature of the ethanol solution rose from 25.2 °C to 39.9 °C. After one fold, it increased from 25.1 °C to 31.5 °C, and after two folds, it rose from 25.2 °C to 29.7 °C. With three folds, it only increased from 25 °C to 27.3 °C. On the other hand, increasing the thickness of the BGNRs@SiO_2/PVDF film at the same particle concentration (figure 4(d)) did not show substantial changes. The final temperatures after ten minutes for three different thicknesses of BGNRs@SiO_2/PVDF films were 32.8 °C, 31.9 °C, and 31.4 °C, respectively. Similar trends were observed when adjusting the thickness of the BGNRs@SiO_2/PDMS film (figure S11). Although the photothermal performance increased with the thickness of the BGNRs@SiO_2/PVDF film due to the thickness increase, this enhancement was solely attributed to the film thickness. The particle concentration remained constant, indicating that particle concentration played a dominant role in this photothermal test. Increasing film thickness under the same particle concentration might enhance photothermal performance, but the effect was not as pronounced as the increase in particle concentration. Compared to the PVDF films prepared by Ding *et al* [38] with gold nanoparticles, our study not only achieves adjustable and predictable bandwidths and peak positions, but also delves deeper into the effects of folding and thickness variations on the photothermal performance of BGNRs@SiO_2/PVDF films.

FDTD simulations

We employed the finite difference time domain (FDTD) method to calculate the extinction spectra of GNRs@SiO_2 in different arrangements. The FDTD simulations were performed using Lumerical commercial software. Figure S12 displays the

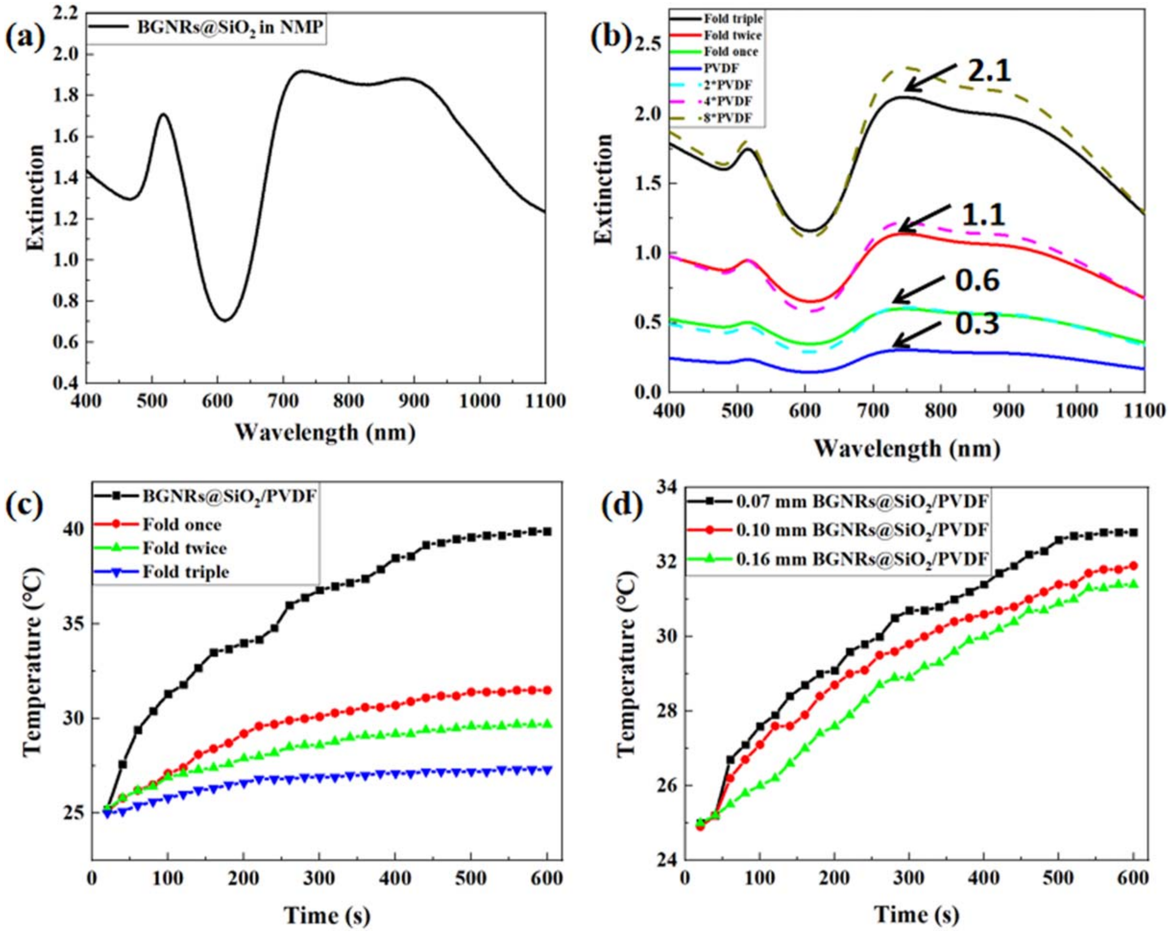

Figure 4. (a) Extinction spectra of BGNRs@SiO_2 mixed with five GNRs in NMP. (b) The solid line represents the measured folded extinction spectrum of the BGNRs@SiO_2/PDVF film, with the peak indicated by the arrow at 740 nm. Meanwhile, the dashed line corresponds to the spectrum of the BGNRs@SiO_2/PDVF film estimated based on the respective coefficients. (c) The temperature variation curves of ethanol under BGNRs@SiO_2/PVDF films without folding (in black), folded once (in red), folded twice (in green), and folded three times (in blue) under 350 W Xenon lamp irradiation over time. (d) The temperature variation curves of ethanol under 0.07 mm BGNRs@SiO_2/PVDF film (in black), 0.10 mm BGNRs@SiO_2/PVDF film (in red), and 0.16 mm BGNRs@SiO_2/PVDF film (in green) under 350W Xenon lamp irradiation over time.

extinction spectra of a single GNR calculated by FDTD based on the measured size, and the LSPR peak of each GNR aligned with the measured extinction spectrum. To simplify the complex configurations, several possible arrangement modes were constructed using six different types of GNRs@SiO_2, as depicted in figures S13–S17. Multiple arrangements were compared in different orientations for each type of GNRs@SiO_2 to calculate the spectra between GNRs@SiO_2, assuming minimal plasmonic coupling after silica coating. Figure 5(a) illustrates the extinction spectra obtained through FDTD calculations, where the full width half maximum (FWHM) could be adjusted from 250 nm to over 492 nm (the arrangements of the GNRs are shown in figure S13). Figure 5(b) shows the measured extinction spectra, with FWHM ranging from 213 nm to over 420 nm (table S2). A comparison between the simulated and measured extinction spectra reveals that the simulated spectra cannot be as flat as the experimental ones due to the monodispersity of the simulated GNRs. Conversely, the measured extinction spectra of GNRs can exhibit relatively flat profiles. The trend observed in the FDTD simulation results aligns with the actual measurement results, indicating that the bandwidths can be adjusted based on the peak position of the added GNRs during mixing. According to figure S14 and figure S15, FDTD simulations demonstrate that the peak position of the extinction spectra is solely dependent on the peak position of the added GNR, regardless of whether the GNRs are arranged horizontally or vertically. Increasing the proportion of GNRs also leads to an increase in the corresponding peak value (figure S16). To approach the real scenarios more closely, we introduced a certain degree of rotation to the gold nanorods to simulate various possible arrangements in the solution (figure S17(a)). It can be observed that the spectral shape undergoes some changes when the nanorods are rotated by certain angles (figure S17(b)). However, when multiple nanorods are rotated at different angles, the spectra almost maintain consistency with those in the horizontal orientation (figure S17(c)). This indicates that in a solution where a large number of nanorods are randomly arranged, theoretical arrangements are unlikely to significantly impact the final results.

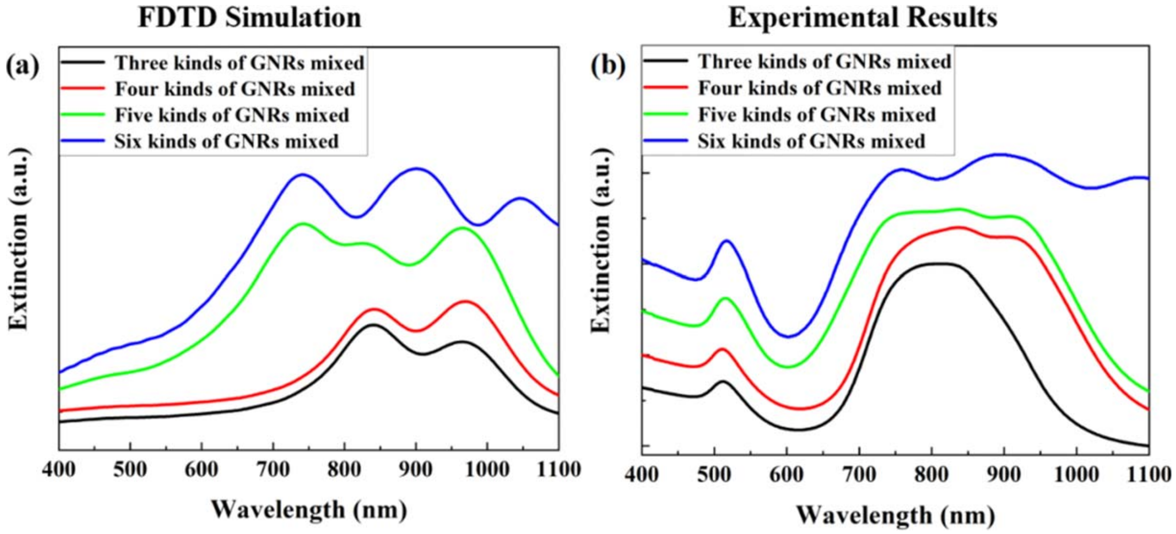

Figure 5. The FDTD simulation (a) and the experimental extinction spectra (b) are shown as BGNRs obtained by mixing three kinds of GNRs (black), four kinds of GNR_S (red), five kinds of GNR_S (green) and six kinds of GNR_S (blue), respectively. The intensity of the spectrum has been offset for clarity.

Conclusion

In summary, this research achieved predictable and adjustable bandwidths in a wide visible-NIR/SWIR spectrum window ($\lambda = 600$ to >1100 nm) by using silica-coated GNRs of different sizes. These GNRs@SiO_2 were then mixed with PDMS or PVDF to form BGNRs@SiO_2/PDMS or BGNRs@SiO_2/PVDF films. The shape of the extinction spectra remained unchanged after the formation of the films. Under Xenon lamp irradiation, the BGNRs@SiO_2/PDMS films exhibited significantly better photothermal performance compared to the PDMS films without particles. The temperature change in the ethanol solution with the BGNRs@SiO_2/PDMS film was only 4 °C, while it was 11.4 °C for the ethanol solution under the PDMS film without particles. Additionally, the extinction spectra of BGNRs@SiO_2/PVDF films remained linear even after folding. Furthermore, the photothermal performance of the folded BGNRs@SiO_2/PVDF film was significantly improved (temperature increase of 14.7 °C without folding and only 2.3 °C after folding three times). Simultaneously, minor variations were observed in adjusting the film thickness (a final temperature difference of only 1.4 °C). This reaffirmed the crucial role of particle concentration in photothermal performance, surpassing the impact of film thickness. The FDTD simulations and experimental results confirmed that the bandwidths of the extinction spectra were adjustable. The presence of large spacing between GNRs (>100 nm) eliminated the plasmonic coupling effect, indicating that the arrangement of the GNRs did not affect the extinction spectra. The shape of the extinction spectra was solely related to the extinction spectra of the added GNRs. Furthermore, the specific arrangement of the GNRs did not influence the final results. This work presents a method to prepare BGNRs@SiO_2 with predictable and adjustable extinction spectra and demonstrates the fabrication of BGNRs@SiO_2/PDMS and BGNRs@SiO_2/PVDF films while preserving their original characteristics. These findings open up broader possibilities for applications in the fields of photothermal conversion and novel optoelectronic devices.

Acknowledgments

The authors thank Sudan Shen for her assistance in TEM at State Key Laboratory of Chemical Engineering (Zhejiang University). The authors also acknowledge financial support from National Natural Science Foundation of China (NSFC, Grant: 61905056). This work was also supported by National Key R&D Program of China (Grant: 2018YFE0207500), the National Natural Science Foundation (Grant 91938201 and 61871169), Zhejiang Provincial Natural Science Foundation (Grant LZ20F010004) and Project of Ministry of Science and Technology (Grant D20011).

Data availability statement

All data that support the findings of this study are included within the article (and any supplementary files).

Supporting information

Supplementary material (Additional experimental and the fitting process of broadband, film preparation process, FDTD simulated extinction spectra) is available in the online version of this article at.

Author information

Notes. The authors declare no competing financial interest.

ORCID iDs

Xi Chen https://orcid.org/0000-0003-4215-1344

References

[1] Ye X, Zheng C, Chen J, Gao Y and Murray C B 2013 Using binary surfactant mixtures to simultaneously improve the dimensional tunability and monodispersity in the seeded growth of gold nanorods *Nano Lett.* **13** 765–9

[2] Ye W *et al* 2020 CTAB stabilizes silver on gold nanorods *Chem. Mater.* **32** 1650–6

[3] Wang H, Wang L, Lin D, Feng X, Niu Y, Zhang B and Xiao F-S 2021 Strong metal–support interactions on gold nanoparticle catalysts achieved through Le Chatelier's principle *Nat. Catal.* **4** 418–24

[4] Liu X Y, Wang J Q, Ashby C R Jr, Zeng L, Fan Y F and Chen Z S 2021 Gold nanoparticles: synthesis, physiochemical properties and therapeutic applications in cancer *Drug Discov. Today* **26** 1284–92

[5] Deng T S, van der Hoeven J E S, Yalcin A O, Zandbergen H W, van Huis M A and van Blaaderen A 2015 Oxidative etching and metal overgrowth of gold nanorods within mesoporous silica shells *Chem. Mater.* **27** 7196–203

[6] Zhao Y Q, Sun Y, Zhang Y, Ding X, Zhao N, Yu B, Zhao H, Duan S and Xu F J 2020 Well-defined gold nanorod/polymer hybrid coating with inherent antifouling and photothermal bactericidal properties for treating an infected hernia *ACS Nano* **14** 2265–75

[7] Yougbare S, Chou H L, Yang C H, Krisnawati D I, Jazidie A, Nuh M and Kuo T R 2021 Facet-dependent gold nanocrystals for effective photothermal killing of bacteria *J. Hazard. Mater.* **407** 124617

[8] Liu S, Zhou X, Zhang H, Ou H, Lam J W Y, Liu Y, Shi L, Ding D and Tang B Z 2019 Molecular motion in aggregates: manipulating TICT for boosting photothermal theranostics *J. Am. Chem. Soc.* **141** 5359–68

[9] Liao J, Shi K, Jia Y, Wu Y and Qian Z 2021 Gold nanorods and nanohydroxyapatite hybrid hydrogel for preventing bone tumor recurrence via postoperative photothermal therapy and bone regeneration promotion *Bioact Mater.* **6** 2221–30

[10] Jia H, Du A, Zhang H, Yang J, Jiang R, Wang J and Zhang C Y 2019 Site-selective growth of crystalline ceria with oxygen vacancies on gold nanocrystals for near-infrared nitrogen photofixation *J. Am. Chem. Soc.* **141** 5083–6

[11] Wei M Z, Deng T S, Zhang Q, Cheng Z and Li S 2021 Seed-mediated synthesis of gold nanorods at low concentrations of CTAB *ACS Omega* **6** 9188–95

[12] Jessl S, Tebbe M, Guerrini L, Fery A, Alvarez-Puebla R A and Pazos-Perez N 2018 Silver-assisted synthesis of gold nanorods: the relation between silver additive and iodide impurities *Small* **14** 1703879

[13] Naik S S, Lee S J, Theerthagiri J, Yu Y and Choi M Y 2021 Rapid and highly selective electrochemical sensor based on ZnS/Au-decorated F-multi-walled carbon nanotube nanocomposites produced via pulsed laser technique for detection of toxic nitro compounds *J. Hazard. Mater.* **418** 126269

[14] Hu B, Sun D W, Pu H and Wei Q 2020 Rapid nondestructive detection of mixed pesticides residues on fruit surface using SERS combined with self-modeling mixture analysis method *Talanta* **217** 120998

[15] Cho H, Moreno-Hernandez I A, Jamali V, Oh M H and Alivisatos A P 2021 *In Situ* quantification of interactions between charged nanorods in a predefined potential energy landscape *Nano Lett.* **21** 628–33

[16] Sutter E, Zhang B and Sutter P 2021 Single-strand DNA-nanorod conjugates - tunable anisotropic colloids for on-demand self-assembly *J. Colloid Interface Sci.* **586** 847–54

[17] Chen Y S, Zhao Y, Yoon S J, Gambhir S S and Emelianov S 2019 Miniature gold nanorods for photoacoustic molecular imaging in the second near-infrared optical window *Nat. Nanotechnol.* **14** 465–72

[18] He T, Jiang C, He J, Zhang Y, He G, Wu J, Lin J, Zhou X and Huang P 2021 Manganese-dioxide-coating-instructed plasmonic modulation of gold nanorods for activatable duplex-imaging-guided nir-ii photothermal-chemodynamic therapy *Adv. Mater.* **33** 2008540

[19] Tang H, Xu X, Chen Y, Xin H, Wan T, Li B, Pan H, Li D and Ping Y 2021 Reprogramming the tumor microenvironment through second-near-infrared-window photothermal genome editing of PD-L1 mediated by supramolecular gold nanorods for enhanced cancer immunotherapy *Adv. Mater.* **33** 2006003

[20] Ostovar B, Cai Y Y, Tauzin L J, Lee S A, Ahmadivand A, Zhang R, Nordlander P and Link S 2020 Increased intraband transitions in smaller gold nanorods enhance light emission *ACS Nano.* **14** 15757–65

[21] Shao W *et al* 2020 Symmetry breaking in monometallic nanocrystals toward broadband and direct electron transfer enhanced plasmonic photocatalysis *Adv. Funct. Mater.* **31** 2006738

[22] Zhao M and Chen P 2020 Exploring plasmonic photocatalysis via single-molecule reaction imaging *Nano Lett.* **20** 2939–40

[23] Huang J, Liu C, Zhu Y, Masala S, Alarousu E, Han Y and Fratalocchi A 2016 Harnessing structural darkness in the visible and infrared wavelengths for a new source of light *Nat. Nanotechnol.* **11** 60–8

[24] Zhou L, Tan Y L, Ji D X, Zhu B, Zhang J X, Gan Q Q, Yu Z F and Zhu J 2016 Self-Assembly of highly efficient, broadband plasmonic absorbers for solar steam generation *Sci. Adv.* **2** e1501227

[25] Chen X, Xu W, Shi Z, Ji Y, Lyu J, Pan G, Zhu J, Tian Y, Li X and Song H 2021 PlasmonicGold nanorods decorated Ti_3C_2 MXene quantum dots-interspersed nanosheet for full-spectrum photoelectrochemical water splitting *Chem. Eng. J.* **426** 130818

[26] Ghosh P, Kar A, Khandelwal S, Vyas D, Mir A Q, Chakraborty A L, Hegde R S, Sharma S, Dutta A and Khatua S 2019 Plasmonic CoO-Decorated Au nanorods for photoelectrocatalytic water oxidation *ACS Appl. Nano Mater.* **2** 5795–803

[27] Jiang W, Wu X, Chang J, Ma Y, Song L, Chen Z, Liang C, Liu X and Zhang Y 2020 Integrated hetero-nanoelectrodes for plasmon-enhanced electrocatalysis of hydrogen evolution *Nano Res.* **14** 1195–201

[28] Chen H Y, Ghosh S, Ponnusamy V K and Chattopadhyay S 2021 Graphene oxide as broadband hyperthermic agent and chemo-photothermal dissolution of kidney-stone mimicking calcium oxalate crystals *J. Photochem. Photobiol.* A **405** 112917

[29] Dey P, Tabish T A, Mosca S, Palombo F, Matousek P and Stone N 2020 Plasmonic nanoassemblies: tentacles beat satellites for boosting broadband NIR plasmon coupling providing a novel candidate for SERS and photothermal therapy *Small* **16** 1906780

[30] Liang J, Liu H, Yu J, Zhou L and Zhu J 2019 Plasmon-enhanced solar vapor generation *Nanophotonics* **8** 771–86

[31] Hong K T, Moon C W, Suh J M, Lee T H, Kim S I, Lee S and Jang H W 2019 Daylight-induced metal-insulator transition in ag-decorated vanadium dioxide nanorod arrays *ACS Appl. Mater. Interfaces* **11** 11568–78

[32] Sah P T, Chang W C, Chen J H, Wang H H and Chan L H 2018 Bimetallic Ag–Au–Ag nanorods used to enhance efficiency of polymer solar cells *Electrochim. Acta* **259** 293–302

[33] Xiang H, Hu Z, Xin C, Lin H J, Aigouy L, Chen Z, Zhou L and Yuan X 2021 Plasmon coupled colloidal gold nanorods for near-infrared and short-wave-infrared broadband photodetection *Adv. Mater. Technol.* **7** 2101217

[34] Kwon N, Oh H, Kim R, Sinha A, Kim J, Shin J, Chon J W M and Lim B 2018 Direct chemical synthesis of plasmonic black colloidal gold superparticles with broadband absorption properties *Nano Lett.* **18** 5927–32

[35] Pastoriza-Santos I, Pérez-Juste J and Liz-Marzán L M 2006 Silica-coating and hydrophobation of CTAB-stabilized gold nanorods *Chem. Mater.* **18** 2465–7

[36] Rowe L R, Chapman B S and Tracy J B 2018 Understanding and controlling the morphology of silica shells on gold nanorods *Chem. Mater.* **30** 6249–58

[37] Zhou N, Polavarapu L, Wang Q and Xu Q H 2015 Mesoporous SnO_2-coated metal nanoparticles with enhanced catalytic efficiency *ACS Appl. Mater. Interfaces* **7** 4844–50

[38] Ding S Y, Zhang J X, Liu C, Li N, Zhang S D, Wang Z Y and Xi M 2022 Investigation of plasmonic-enhanced solar photothermal effect of Au NR@PVDF micro-/nanofilms *ACS Omega* **7** 20750–60